Electronic Supplementary Material (ESI) for Lab on a Chip.

Supplementary Information

Nano-Injection Molding with Resin Mold Inserts for Prototyping of Nanofluidic Devices for Single Molecular Detection

Farhad Shiri,[1,2‡] Junseo Choi,[2,4‡] Chad Vietz, [1,2‡] Chathurika Rathnayaka,[1,2] Anishkumar Manoharan,[1,2] Suresh Shivanka,[1,2] Guoqiang Li,[4] Chengbin Yu,[4] Michael C. Murphy,[2,4] Steven A. Soper,[1,2,3,5,6,7*] and Sunggook Park,[2,4*]

[1]Department of Chemistry, The University of Kansas, Lawrence, KS 66045

[2]Center of BioModular Multiscale Systems for Precision Medicine

[3]Bioengineering Program, The University of Kansas, Lawrence, KS 66045

[4]Mechanical & Industrial Engineering Department, Louisiana State University, Baton Rouge, LA 70803

[5]Department of Mechanical Engineering, The University of Kansas, Lawrence, KS 66045

[6]KU Cancer Center, University of Kansas Medical Center, Kansas City, KS 66160

‡These authors contributed equally to this manuscript.

*Authors to whom correspondence should be addressed.

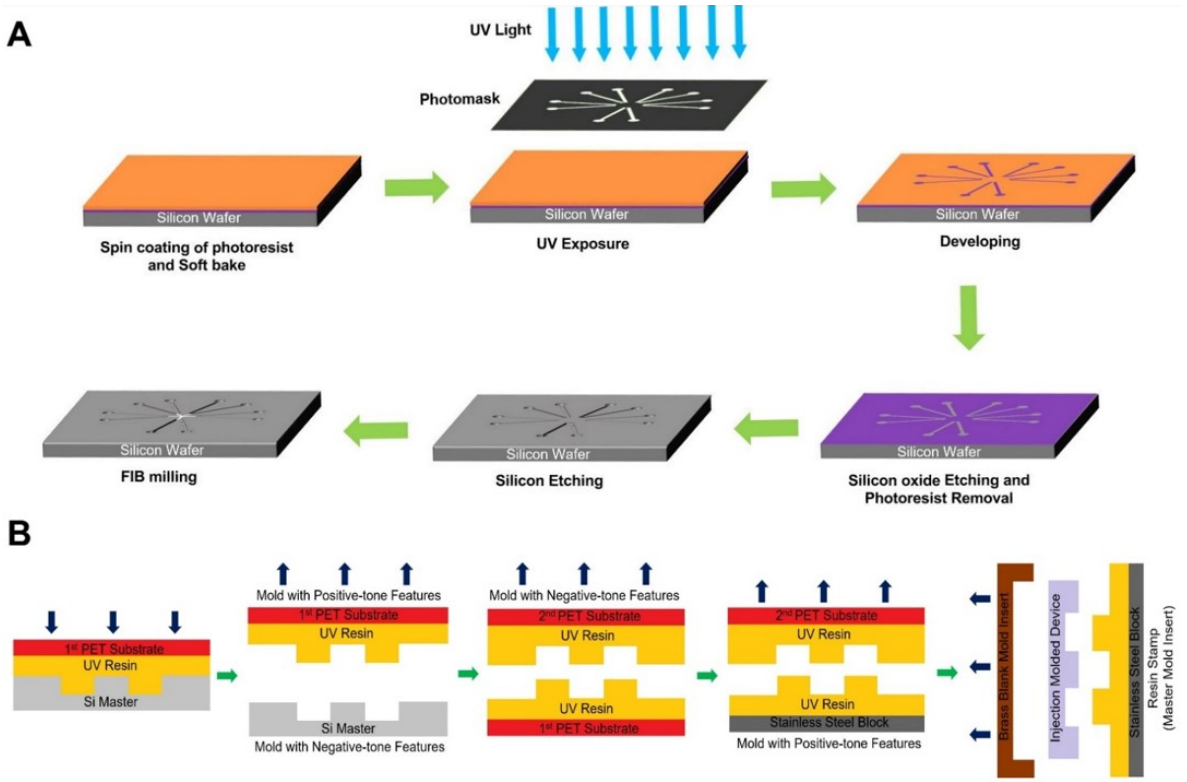

Figure S1. (A) Schematic representation of Si master fabrication using photolithography, dry or wet etching, and FIB milling to generate the required nanostructures. (B) Schematics of the various micro/nanopattern transfers from the Si master to the final UV resin mold insert. Depending on the required polarity of structures, pattern transfer was performed either once or twice. The final resin mold insert consisted of a patterned UV resin layer sitting on top of a stainless-steel block that was fit into the multi-unit die (MUD) used for injection molding.

Table S1. Properties of three UV resins used for UV resin mold inserts (1).

UV-Resin	Molecular weight (g/mol)	Viscosity of UV-resin solution (cps)	Youngs modulus of cured UV resin (MPa)	Surface energy of cured UV resin (mN/m)
PUA	600-6000	241.4	4771	60
TPGDA	300	N/A, but lower than PUA and MD700	698	24.76
MD 700	1600	850	10.5	12.7

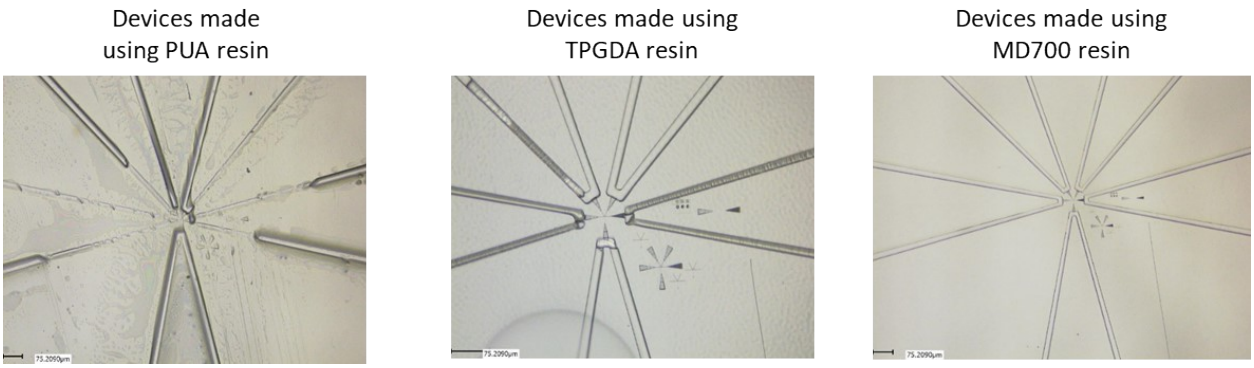

Figure S2. Optical micrographs of injection molded COP substrates using three different resin mold inserts. Identical injection molding conditions were used for these experiments; T_{nozzle} = 270 °C and T_{mold} = 60 °C.

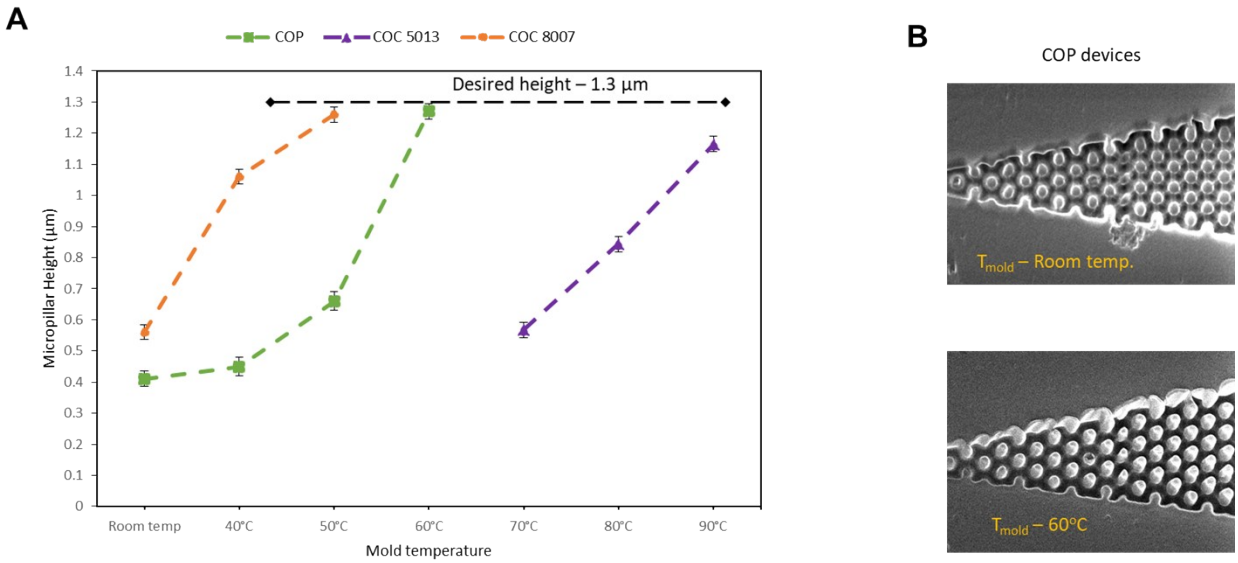

Figure S3. (**A**) Graph showing differences in micropillar heights of devices molded using various thermoplastics (COC 8007, COC 5013 and COP). Despite the ability to replicate the associated nanochannels within the fluidic device, micropillar (1.3 µm) height was taken into consideration to determine the replication fidelity. Micropillars replicated using COC 8007 and COP thermoplastics generated up to 97% of the micropillar height at mold temperatures of 50 °C and 60 °C, respectively. Using COC 5013, a pillar height up to 90% of the Si master height was achieved even at a mold temperature of 90 °C. (**B**) Scanning electron micrographs of injection molded micropillars formed in COP at two mold temperatures (room temperature and 60 °C).

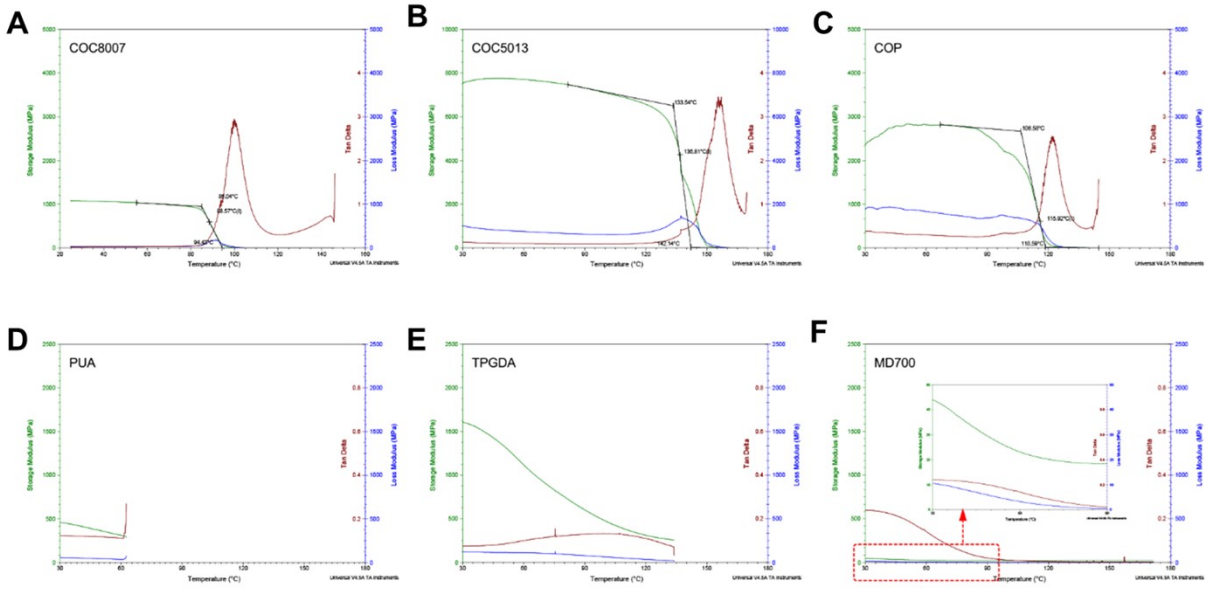

G

Thermoplastics for injection molding	Storage modulus at RT (MPa)	T_g determined by storage modulus (°C)	Cured resins for resin molds	Storage modulus at RT (MPa)	Storage modulus 60 °C (MPa)	Storage modulus at 100 °C (MPa)
COC 8007	1077	89	PUA	469	316	n/a
COC 5013	7765	137	TPGDA	1625	1114	476
COP	2832	116	MD 700	45	23	18

Figure S4. (**A**) Graphs showing storage modulus, loss modulus, and tan δ of different polymers used in this study. The measurements were performed by dynamic mechanical analysis using a Q-800 dynamic mechanical analyzer (TA instruments). (**A-C**) correspond to three thermoplastics used for injection molding and (**D-F**) show results for three cured UV resins used for resin molds. (**G**) Table showing the storage modulus values at room temperature and the glass transition temperature (T_g) determined by storage modulus curves.

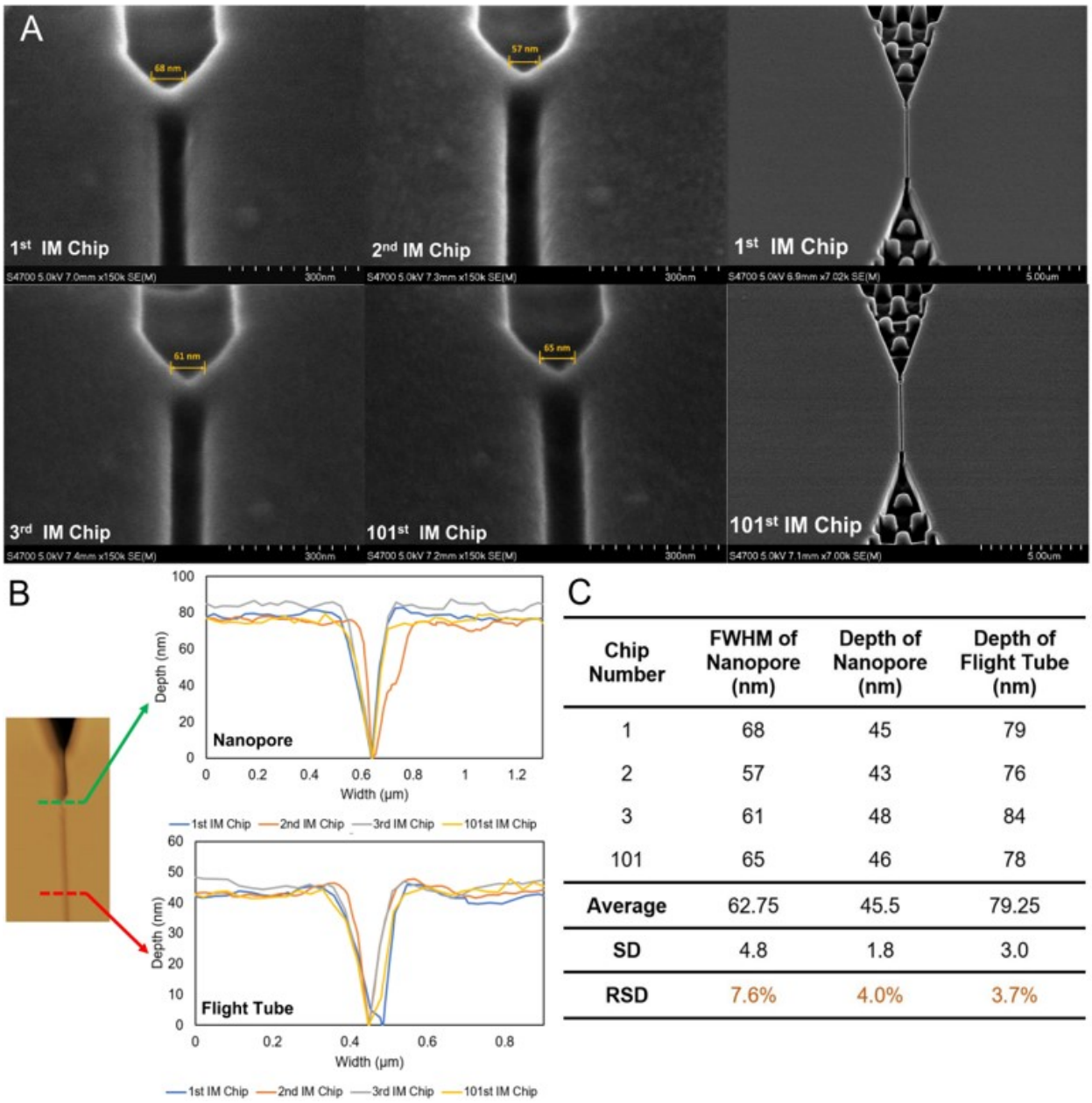

C

Chip Number	FWHM of Nanopore (nm)	Depth of Nanopore (nm)	Depth of Flight Tube (nm)
1	68	45	79
2	57	43	76
3	61	48	84
101	65	46	78
Average	62.75	45.5	79.25
SD	4.8	1.8	3.0
RSD	7.6%	4.0%	3.7%

Figure S5. (A) Scanning Electron Microscopy (SEM) images depicting injection molded (IM) dual in-plane nanopore chips: Representing the 1st, 2nd, 3rd, and 101st iterations of IM chips. The images in the left and middle columns highlight the nanopore and flight tube regions, while the images in the right column focus on the flight tube and funnel section. (B) Left: Atomic force microscopy (AFM) image of an in-plane nanopore IM chip. Top: cross-sectional profiles of IM chips in the nanopore region for the 1st, 2nd, 3rd, and 101st iterations of IM chips. Bottom: cross-sectional profiles of IM chips in the nanochannel flight tube region for the same iterations. (C) The inset table presents the critical dimensions including full width at half maximum (FWHM) of the nanopore, depths of the nanopores and nanochannel flight tube for the 1st, 2nd, 3rd, and 101st iterations of IM chips.

Table S2. Injection molding conditions for nanofluidic devices shown in **Figure 1C** (X-ToF device) formed in different thermoplastic substrates. The X-ToF device consists of a central solid phase nanoreactor, five nanochannels, and a microfluidic network.

Molding material	T_g (°C)	T_{nozzle} (°C)	T_{mold} (°C)	Injection speed (cm^3/s)	Dosage (cm^3)	Cooling time (s)
COC 8007	78	230	50	10	4.2	30
COC 5013	134	270	90	10	2.8	60
COP	100	260	60	10	3.7	30

Table S3. Comparison of injection molding conditions with a COP substrate for two different nanofluidic devices used in this work. The dual in-plane nanopore sensor shown in **Figure 1B** consists of 2 in-plane pores located at either end of the nanochannel fight tube. The X-ToF device consists of structures as delineated in **Table S2**.

	T_{nozzle} (°C)	T_{mold} (°C)	Injection speed (cm^3/s)	Dosage (cm^3)	Cooling time (s)
Dual nanopore sensor	270	60	5	3.9	30
XTOF device	260	60	10	3.7	30

References

1. Jia, Z., Choi, J. and Park, S. (2018) Selection of UV-resins for nanostructured molds for thermal-NIL. *Nanotechnology*, **29**, 365302.